Gravity-driven thin film flow: the influence of topography and surface tension gradient on rivulet formation

D. Slade[1*], S. Veremieiev[1], Y.C. Lee[2] and P.H. Gaskell[1]

[1] *School of Mechanical Engineering, University of Leeds, Leeds, LS2 9JT, UK*

[2] *Department of Mechanical Engineering, Heriot-Watt University, Edinburgh, EH14 4AS, UK*

[*] *Corresponding author: mndsl@leeds.ac.uk*

Abstract

The evolution of an advancing fluid front formed by a gravity-driven thin film flowing down a planar substrate is considered, with particular reference to the presence of Marangoni stresses and/or surface topography. The system is modelled using lubrication theory and solved via an efficient, adaptive multigrid method that incorporates automatic, error-controlled grid refinement/derefinement and time stepping. The detailed three dimensional numerical results obtained reveal that, for the problems investigated, while both of the above features affect the merger of rivulets by either delaying or promoting the same, topography influences the direction of growth.

Keywords: thin film, rivulet, lubrication theory, Marangoni stress, topography

1. Introduction

Thin film flows over substrate containing heterogeneities in the form of micro-scale topographical irregularities arise in many naturally occuring biological, medical and industrial processes [1]. The resulting complex and interesting fluid dynamics involved, as well as the stability of the advancing front formed by a spreading film, make the topic of rivulet formation in particular both important and fascinating. The observed formation of rivulets on an inclined homogeneous substrate was first reported by Huppert [2], who recorded that the advancing front became unstable leading to the development of periodic rivulets that grew in time. There have been many subsequent investigations, mainly numerical, of the phenomenon; for example Diez and Kondic [3] explored gravity-driven flow on inclined planar and patterned substrates, discovering that the inclination angle affects the shape and length of the rivulet patterns formed. Cazabat *et al.* [4] investigated experimentally the case of a film driven, in opposition to gravity, by thermal gradients and found that, in a similar way to gravity-driven films, rivulets form at the advancing front - the surface tension gradients present having a large influence on the associated dynamics. Eres *et al.*[5] developed a model to replicate their experimental set up and predicted the break up of the associated rivulets at low velocities.

Kondic and Diez [6] investigated the affect of small perturbations in the substrate on a stable front; the resulting rivulet formation was found to be very similar to that observed when contact line perturbations are applied to the advancing front. The use of striped substrates in the control of rivulet spacing has also been investigated, Kondic and Diez [7]. Zhao and Marshall [8] modelled the chemical heterogeneity of a substrate by varying the contact angle the fluid makes with it; striped surfaces are reported to provide a means of controlling the wavelength of the emerging rivulets, either widening or decreasing the spacing between them.

The focus of the present work is that of a fully wetting, three dimensional, gravity-driven thin film, encompassing flow on planar substrates and ones containing microscale topographies. Also considered are Marangoni effects, which can arise when thermal gradients are present. The flow behaviour is modelled via lubrication theory; the associated equation set governing the evolving flow is solved accurately using an efficient multigrid methodology, incorporating both error controlled, automatic space and time adaptivity - the first time such flows have been solved in this manner.

2. Problem formulation

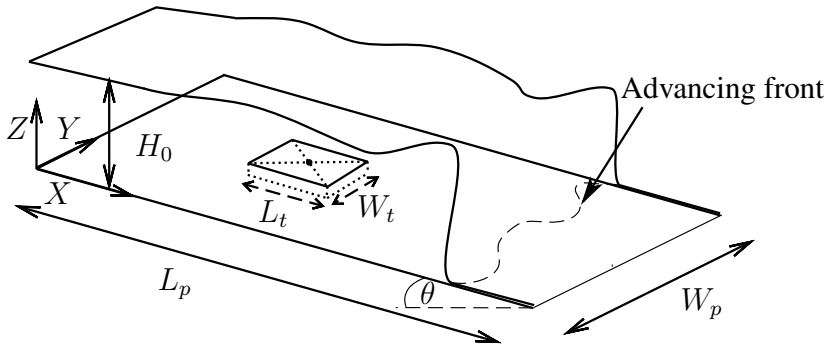

Figure 1: Schematic diagram of rivulet flow down an inclined planar substrate containing rectangular topography (height/depth S_0, width, W_t, and length, L_t).

The problem of interest is shown schematically in Figure 1. It consists of a thin fluid film of thickness H, flowing down a substrate (width, W_p, length, L_p) inclined at angle θ to the horizontal; the volumetric flow rate is Q_0 per unit width. The fluid is considered to be incompressible with constant density, ρ, and viscosity, μ, and variable surface tension, σ, given by $\sigma = \sigma_0\tilde{\sigma} = \sigma_0 + \tau X$ with σ_0 the value of surface tension at $X = 0$ and $\tau\,(= \partial\sigma/\partial X)$ a constant surface tension gradient [4]. The film is considered to be fully wetting; a precursor film of thickness, H^*, located ahead of the advancing front, alleviates the singularity associated with the attendant contact line [6, 8, 9]. The long-wave approximation is invoked on the assumption that the asymptotic film thickness, H_0, is small compared to the capillary length, $L_0 = H_0/(6Ca)^{\frac{1}{3}}$, where $Ca = \mu U_0/\sigma_0 \sim O\left(\epsilon^3\right) \ll 1$ is the capillary number, that is $H_0/L_0 = \epsilon \ll 1$; the characteristic velocity $U_0 = 3Q_0/2H_0$. In which case, together with the introduction of the following scalings [10]:

$$(x, y) = \frac{(X, Y)}{L_0}, \quad z = \frac{Z}{H_0}, \quad h\,(x, y, t) = \frac{H\,(X, Y, T)}{H_0}, \quad t = \frac{U_0 T}{L_0}, \quad s\,(x, y) = \frac{S\,(X, Y)}{H_0}$$
$$p\,(x, y, z, t) = \frac{2P\,(X, Y, Z, T)}{\rho g L_0 \sin\theta}, \quad (u, v, w) = \left(\frac{U}{U_0}, \frac{V}{U_0}, \frac{W}{\epsilon U_0}\right), \quad h^* = \frac{H^*}{H_0},$$

the Navier-Stokes and continuity equations, for no slip at the substrate together with the usual free-surface stress and kinematic boundary conditions [11], reduce to the following coupled equation set:

$$\frac{\partial h}{\partial t} = \frac{\partial}{\partial x}\left[\frac{h^3}{3}\left(\frac{\partial p}{\partial x} - 2\right) - \frac{\tilde{\tau} h^2}{2}\right] + \frac{\partial}{\partial y}\left[\frac{h^3}{3}\left(\frac{\partial p}{\partial y}\right)\right], \tag{1}$$

$$p = -\frac{\epsilon^3}{Ca}\hat{\sigma}\nabla^2\,(h + s) + 2\epsilon\,(h + s - z)\cot\theta, \tag{2}$$

where $h, p, \tilde{\tau}\ (= H_0\tau\ /\ \mu U_0)$ and s are the dimensionless film height, pressure, constant surface tension gradient and topography height/depth, respectively. The topography, $s(x, y)$, with height (depth) $s_0 = S_0/H_0 > 0$ ($s_0 < 0$), length

$l_t = L_t/L_0$ and width $w_t = W_t/L_0$, defined using arctangent functions [12], takes the form:

$$s\left(x,y\right) = \frac{s_0}{b_0}\left[\tan^{-1}\left(\frac{x - x_t - \frac{l_t}{2}}{\gamma l_t}\right) + \tan^{-1}\left(\frac{x_t - x - \frac{l_t}{2}}{\gamma l_t}\right)\right] \times \left[\tan^{-1}\left(\frac{y - y_t - \frac{w_t}{2}}{\gamma w_t}\right) + \tan^{-1}\left(\frac{y_t - y - \frac{w_t}{2}}{\gamma w_t}\right)\right] \quad (3)$$

with the centre of the topography at (x_t, y_t). The steepness of the topography is controlled by γ with:

$$b_0 = 4\left[\tan^{-1}\left(\frac{1}{2\gamma}\right)\right]^2. \quad (4)$$

When topographies are present, they are restricted to simple square peak and trench features with $\gamma = 0.01$.

At the upstream boundary a fully developed film thickness is prescribed ($h = 1$) while the downstream boundary is set such that $h(l_p, y) = h^*$ with zero flux conditions defined for h and p at the other boundaries, namely:

$$\left.\frac{\partial h}{\partial x}\right|_{x=0} = \left.\frac{\partial p}{\partial x}\right|_{x=0} = \left.\frac{\partial h}{\partial x}\right|_{x=l_p} = \left.\frac{\partial p}{\partial x}\right|_{x=l_p} = 0,$$

$$\left.\frac{\partial p}{\partial y}\right|_{y=0} = \left.\frac{\partial p}{\partial y}\right|_{y=w_p} = \left.\frac{\partial h}{\partial y}\right|_{y=0} = \left.\frac{\partial h}{\partial y}\right|_{y=w_p} = 0.$$

where $l_p = L_p/L_0$ and $w_p = W_p/L_0$. The initial film profile consists of a front perturbed with a superposition of N modes with random length, $l_j \in [-0.2, 0.2]$, and differing wavelength, $\lambda_{0,j}$, as in [6] via:

$$h(x,y) = 0.5\left\{1 + h^* - (1 - h^*)\tanh\left[\frac{(x - x_f(y))}{\delta}\right]\right\}, \quad (5)$$

$$x_f\left(y\right) = x_u - \sum_{j=1}^{N} l_j \cos\left(2\pi y/\lambda_{0,j}\right), \quad (6)$$

where x_u is the position of the slope of the unperturbed front, δ is the steepness of the profile (taken here to be 0.01) and $\lambda_{0,j} = 2w_p/j$ for $j = 1, ..., N$. The results are independent of the initial condition provided N is sufficiently large; a value of $N = 50$ is found to be adequate.

3. Method of solution

3.1. Difference equations

Discretising equations (1) and (2) using second order central-differencing [10], remembering that $\tilde{\tau}$ is constant, leads to the following corresponding finite-difference analogues:

$$\frac{\partial h_{i,j}}{\partial t} = \frac{1}{\Delta^2}\left[\frac{h^3}{3}|_{i+\frac{1}{2},j}\left(p_{i+1,j} - p_{i,j}\right) - \frac{h^3}{3}|_{i-\frac{1}{2},j}\left(p_{i,j} - p_{i-1,j}\right) + \frac{h^3}{3}|_{i,j+\frac{1}{2}}\left(p_{i,j+1} - p_{i,j}\right) - \frac{h^3}{3}|_{i,j-\frac{1}{2}}\left(p_{i,j} - p_{i,j-1}\right)\right] - \frac{\tilde{\tau}}{2\Delta}\left(\frac{h^2|_{i+1,j}}{3} - \frac{h^2|_{i-1,j}}{3}\right) - \frac{2}{\Delta}\left(\frac{h^3}{3}|_{i+\frac{1}{2},j} - \frac{h^3}{3}|_{i-\frac{1}{2},j}\right), \quad (7)$$

$$p_{i,j} + \frac{\epsilon^3\hat{\sigma}}{Ca\Delta^2}\left[\left(h_{i+1,j} + s_{i+1,j}\right) + \left(h_{i-1,j} + s_{i-1,j}\right) + \left(h_{i,j+1} + s_{i,j+1}\right) + \left(h_{i,j-1} + s_{i,j-1}\right) - 4h_{i,j}\right] - 2\epsilon\left(h_{i,j} + s_{i,j}\right)\cot\theta = 0, \quad (8)$$

defined at all points (i, j) of the computational domain, $(0, l_p) \times (0, w_p)$; the prefactors are obtained using linear interpolation between neighbouring grid points and are given by, for example,

$$\frac{h^3}{3}|_{i+\frac{1}{2},j} = \frac{1}{2}\left(\frac{1}{3}h^3_{i+1,j} + \frac{1}{3}h^3_{i,j}\right),$$

and similarly for the other prefactors. The mesh size is denoted by Δ and is taken to be the same in both the x and y directions. The time derivatives are discretised via the implicit, second-order Crank Nicolson method.

3.2. Adaptive multigrid solver

Equations (7) and (8) are solved using an efficient multigrid method employing a combined full approximation storage (FAS) algorithm and full multigrid (FMG) strategy, on successively finer grids $G_0, ..., G_K$, where G_0 is the coarsest grid and G_K the finest one, by performing a number of FAS W-cycles on each level. The number of nodes, n_k, on mesh level, k, is given by $n_k = A_x 2^k + 1$ in the x-direction and $m_k = A_y 2^k + 1$ in the y-direction, where A_x and A_y are constant multiplication factors. The main concept of multigridding is to exploit the coarser grid levels in the reduction of errors, thus reducing the work done on the finer grids to maximise efficiency; relaxation is performed via a red-black Gauss-Seidel Newton method. Ghost nodes are assigned to implement Neumann boundary conditions; exact values are assigned at the appropriate boundary points in the case of Dirichlet boundary conditions.

The solution strategy incorporates error-controlled, automatic spatial and temporal adaptivity as described in [10]. Variable time-stepping is implemented by estimating the local truncation error (LTE) at each time step, controlled by a user defined tolerance. The grids automatically refine/de-refine locally so that the resolution is finest in the vicinity of the advancing front and devolves in areas where the solution is smooth and away from any free-surface disturbances. Areas where grid devolution is active are determined by the gradient of the solution; should the gradient be close to zero at a particular node then this node will be removed from subsequent calculations in the current multigrid cycle. These features allow for the efficient and accurate calculation of long time solutions of rivulet growth.

4. Results

The results presented below are for the case of the flow of a 100μm water film (density $\rho = 1000$ kg m^{-3}, viscosity 0.001 Pa s and surface tension $\sigma_0 = 0.07$ N m^{-1}) on a substrate inclined at 65° to the horizontal, this gives $Ca = 6.35 \times 10^{-4}$ and $\epsilon = 0.16$. The precursor film thickness is taken to be $h^* = 0.01$ (1 μm); a value chosen to be consistent with the one used by Diez and Kondic [3]. The initial profile was defined using equation (5) and the front perturbed as per equation (6); to facilitate comparison between the results generated, l_j and $\lambda_{0,j}$ were kept the same.

4.1. *Marangoni effects*

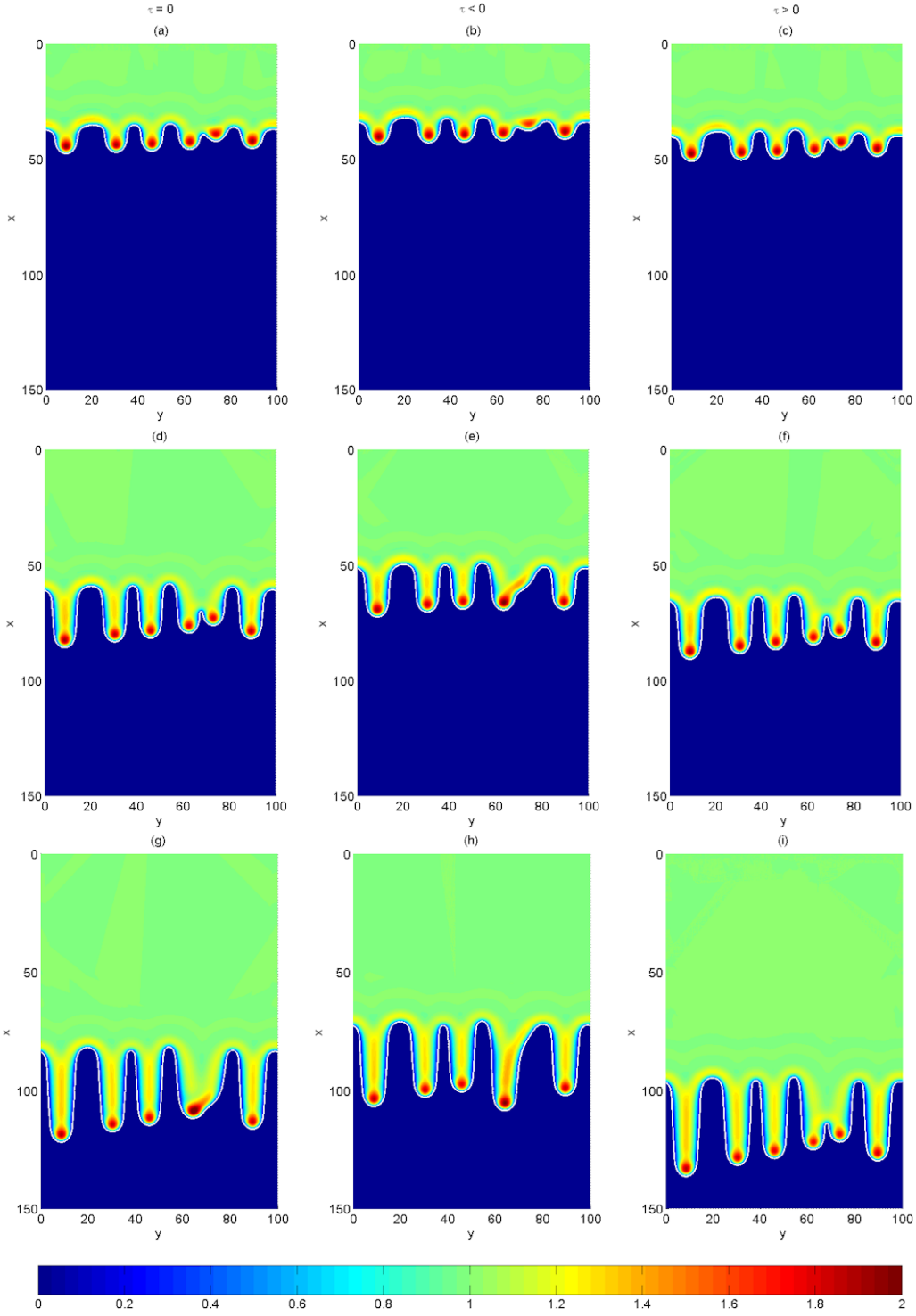

Figure 2: Colour maps of the free surface height, $h + s$, for gravity-driven flow over a planar substrate, $s_0 = 0$, and $\theta = 65°$: the flow pattern at t = 50 (top), t = 100 (middle) and t = 150 (bottom) when $\tilde{\tau} = 0.0$ (left), $\tilde{\tau} = -0.25$ (centre) and $\tilde{\tau} = 0.25$ (right), respectively, in the streamwise direction.

The results shown in Figure 2 were obtained on a computational domain with $(l_p, w_p) = (200, 100)$; the adaptive multigrid method utilised five grid refinement levels, $0 \leq k \leq 4$, with the number of nodes on each level being $n_k = 278 \times 2^k + 1$ and $m_k = 139 \times 2^k + 1$ which equates to a finest mesh resolution of $\Delta = 0.045$. The value of $\tilde{\tau}$ is prescribed as

indicated; surface tension gradients of similar magnitude have been achieved in an experimental setting using heated substrates [4]. Comparing the top and middle set of colour maps reveals the effect of the surface tension gradient, $\tilde{\tau}$, see equation (1), acting in the streamwise direction. The main difference is seen in the length of the rivulets formed: a value of $\tilde{\tau} > 0$ accelerates the growth rate of the rivulets with the spreading rate characterised by an increase in the maximum film height at the capillary ridge at their tips; for $\tilde{\tau} < 0$, the opposite effect is observed and there is a flattening/decrease in the capillary ridge at the tips suppressing the growth rate. At even later times, see the bottom set of colour maps, the difference in position and length is even more pronounced.

The merging of neighbouring rivulets can also be observed in Figure 2 and is similarly affected by the presence of a surface tension gradient. In Figure 2(e), where $\tilde{\tau} < 0$, the merger of two rivulets has just occured with their tips coalescing to form a new, single rivulet; the reduced growth rate of these rivulets mean they interact at an earlier stage and coalesce. The same rivulets in Figure 2 (d) and (f), $\tilde{\tau} \geq 0$, have yet to merge fully but have begun to do so from their common base; they will eventually merge but at a later time. This is seen to have happened in Figure 2(g), for $\tilde{\tau} = 0$; however, with $\tilde{\tau} = 0.25$, Figure 2(i), the rivulet tips remain distinct. The rivulet formed by the merging process, see Figure 2(h), has accelerated ahead of its neighbours due to the increase in capillary ridge height which accompanies a merging and which in turn leads to accelerated growth. A negative surface tension gradient promotes earlier merger of neighbouring rivulets, whereas a positive one delays the time at which merger occurs.

4.2. Topography

Considered next is the effect of the presence of topographical features, located ahead of the advancing front and encountered by the same, where the spacing and topography type influences the resulting flow. An example of this is shown in Figure 3 for the case of an advancing front moving down a smooth planar substrate and one encountering two identical trenches, two identical peaks and equal but opposite trench and peak topographies. All topographies have height $s_0 = |0.2|$ and length and width $l_t = w_t = 10$. The domain size for these solutions is $(l_p, w_p) = (250, 50)$ with, in this case, the number of nodes on level k given by $n_k = 348 \times 2^k + 1$ and $m_k = 70 \times 2^k + 1$.

The upper set of plots in Figure 3 shows the rivulet structures at $t = 100$; the different combinations of topographical features clearly affect the position and growth of the rivulets. When twin trenches are present, as shown in Figure 3(b), the two inner most rivulets formed are slightly longer in length and slightly more advanced of the corresponding rivulets in the planar flow case, Figure 3(a). Figure 3(c), for the case of twin peaks, shows a very different pattern emerging; the inner most rivulets have already merged after being directed towards one another. The merging of the two rivulets is accompanied by a sharp increase in the height of the capillary ridge at the tip of the newly formed single rivulet which leads to an acceleration in growth of the structure.

At later times, see the bottom set of colour maps at $t = 258$, the influence of topography persists. The inner most rivulets have merged in all cases apart from that in which the front encounters twin trenches; this suggests that the increased growth rate experienced in the latter case prevents these rivulets from merging. The middle rivulet in Figure 3 (h) is skewed to the left compared to the ones in Figures 3 (e) and (g) due to the predominant deflection effect of the peak. The centre rivulet in the twin peak topography case, Figure 3 (g), results from the merging that occured at much earlier times so has the usual, elongated shape. The other newly formed, single, centre rivulet, Figure 3 (e) and (h), has a wider,

V-shaped base due to it being fed from the two combined sources of the now merged rivulets. As time progresses, the increase in ridge height at the tip leads to an acceleration of the rivulet front which elongates the structure.

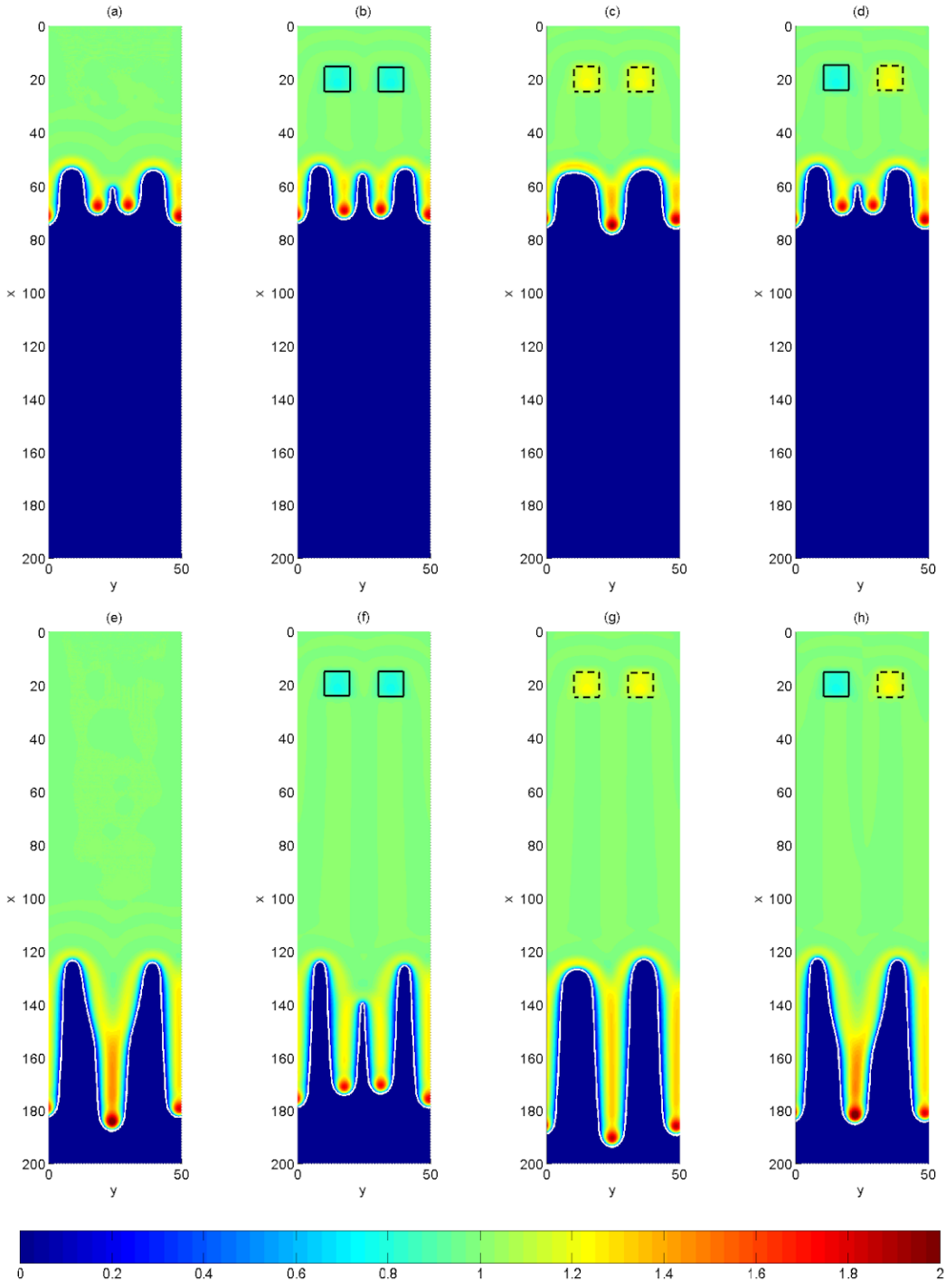

Figure 3: Colour maps of the free surface, $h + s$, showing rivulet formation for flow over substrate containing different topographical heterogeneities, $|s_0| = 0.2$ and $\theta = 65°$, shown at $t = 100$ (top) and $t = 258$ (bottom): the substrate contains (from left to right) no topography; two square trench topographies; two peak topographies (dashed outline); and a square trench and a square peak topography. $\tilde{\tau} = -0.25$ in all cases.

5. Conclusion

Gradients in the surface tension offers a useful tool for controlling the development of gravity-driven rivulets in terms of length and growth rate. The application of a surface tension gradient at the advancing front can be used to suppress or promote rivulet growth. The possibility of applying localised surface tension gradients at strategic points along the advancing front offers the prospect of suppressing rivulet growth almost completely. Topographical features present on the substrate directly affect the symmetry and merger of rivulets; they influence the direction of growth and merging patterns. Peak topographies may deflect the path of a rivulet and can promote merging with one of its neighbours. For flow over trench topographies, rivulet growth is promoted due to the surge experienced [12]. These features point to the possibility of strategic control over the direction and speed of spreading rivulets. It can similarly be shown that if a surface tension gradient is applied perpendicular to the principal direction of flow, the rivulets grow but in a preferential diagonal manner in the direction of the Marangoni stress and that if alternating surface tension gradients are applied at different positions down the length of the substrate, the rivulets can be made to bend.

References

[1] R. V. Craster and O. K. Matar. Dynamics and stability of thin liquid films. *Reviews of Modern Physics*, 81, 2009.

[2] H. E. Huppert. Flow and instability of a viscous current down a slope. *Nature*, 300(5891):427–9, 1982.

[3] J. A. Diez and L. Kondic. Contact line instabilities of thin liquid films. *Physical Review Letters*, 86(4), 2001.

[4] A. M. Cazabat, F. Heslot, S. M. Troian, and P. Carles. Fingering instability of thin spreading films driven by temperature gradients. *Nature*, 346, 1990.

[5] M. H. Eres, L. W. Schwartz, and R. V. Roy. Fingering phenomena for driven coating films. *Physics of Fluids*, 12(6):1278–1295, 2000.

[6] L. Kondic and J. Diez. Pattern formation in the flow of thin films down an incline: Constant flux configuration. *Physics of Fluids*, 13(11):3168–3184, 2001.

[7] L. Kondic and J. Diez. Flow of thin films on patterned surfaces: Controlling the instability. *Physical Review E*, 65(4), 2002.

[8] Y. Zhao and J. S. Marshall. Dynamics of driven liquid films on heterogeneous surfaces. *Journal of Fluid Mechanics*, 559:355–378, 2006.

[9] A. Bertozzi and M. P. Brenner. Linear Stability and Transient Growth in Driven Contact Lines. *Physics of Fluids*, 9:530-539, 1997.

[10] Y. C. Lee, H. M. Thompson, and P. H. Gaskell. An efficient adaptive multigrid algorithm for predicting thin film flow on surfaces containing localised topographic features. *Computers and Fluids*, 36:838–855, 2007.

[11] S. Veremieiev, H. M. Thompson, Y. C. Lee, and P. H. Gaskell. Inertial thin film flow on planar surfaces featuring topography *Computers and Fluids*, 39(3):431–450, 2010.

[12] P. H. Gaskell, P. K. Jimack, M. Sellier, H. M. Thompson, and M. C. T. Wilson. Gravity-driven flow of continuous thin liquid films on non-porous substrates with topography. *Journal of Fluid Mechanics*, 509:253–280, 2004.